

Tests of a High Resolution Time of Flight System Based on Long and Narrow Scintillator

E. Chen, M. Saulnier, W. Sun and H. Yamamoto.
Harvard University, Cambridge, Massachusetts 02138

October 1, 2018

We have tested a prototype time-of-flight system based on bulk scintillator block of dimensions $2.5 \times 2.5 \times 200$ cm³. Using a calibration scheme similar to the one used in actual collider experiments, we have achieved a resolution of 71 ps using Amperex XP2020/UR photomultipliers and 81 ps using proximity-focusing fine-mesh photomultipliers (Hamamatsu R2021). Results are also obtained for scintillating fiber blocks of the same dimensions. Good internal reflectivity of the bulk scintillator block resulted in resolutions superior to the fibre blocks. A single-photon pulsed laser system was used to study photomultipliers and the results were used in a Monte Carlo simulation of the system to study the critical elements that determine the resolution.

1 Introduction

In many high energy physics experiments the identification of particle species is accomplished through time-of-flight (TOF) measurements utilizing a system of plastic scintillators read out by photomultiplier tubes (PMT's). A typical configuration for a detector at a colliding beam facilities is a barrel geometry consisting of a single layer of long rectangular scintillation counters parallel to the beam, segmented in azimuth, and read out at both ends by photomultipliers coupled to light guides [1]. Two important factors that define the performance of such TOF systems are the timing resolution and the efficiency to register a clean hit. Using 2.8 meter long counters of thickness 5 cm and width 10 cm, the CLEO II experiment obtains resolutions of 139 ps for bhabha events and 154 ps for hadronic events [3, 4]. The efficiency for obtaining good timing information for a track is limited primarily by events where two or more particles strike the same counter. In these cases one is no longer able to effectively utilize the timing measurements from both ends, and the resolution is consequently substantially worse. The efficiency at CLEO II for spherical events is approximately 85% and for jetlike events, approximately 75%.

The factors that determine the timing resolution are quite well understood: the number of photoelectrons detected, [2] the dispersion of path length from the scintillation point to the photocathode, the scintillation decay time, and the transit time spread of

the photomultiplier. Thus, one tries to use fast and efficient scintillator with long attenuation length, fast phototubes with small transit time spread covering as much area as possible at the end of the scintillator preferably without any light guides. As a rule of thumb, one loses the precious scintillation photons by a fraction proportional to the ratio of the cross section of the scintillator to the photocathode area. The light guide can add dispersion of photon path length and further photon loss [5]. The lack of light guides usually requires photomultipliers that can operate within a high magnetic field (~ 1 T). The thickness of the scintillator should be as thick as possible as long as other detector requirements are met [6].

The efficiency argues for a fine segmentation. The effective attenuation of a finely segmented system, however, tends to be small due to the increased number of internal reflections. It has been suggested that resolutions for long counters can be improved by using scintillating fibers [8]. The advantage of a fiber counter is that the resolution at large distances is not severely limited by photon path length dispersion and that the loss due to internal reflections are small [7]. On the other hand, fiber counters have a small trapping angle which limits the absolute amount of light collected by the PMT. The authors of reference [8] compared bulk and fiber counters and concluded that the system using the fiber counter has a better resolution at long distances. However, if the effective attenuation length of the bulk counter is made comparable to that of the fiber counter, then the bulk

as it passes through the layers of meshes [14]. The effect (b) is the main reason for gain loss in a high field, while the effect (a) result in higher gains when the PMT axis is at some angle θ (about 30 degrees) with respect to the field than zero angle. The effect (c) is responsible for the sharp drop of gain for θ greater than some value (about 50 degrees). We have not studied fine-mesh PMT's inside high magnetic field. Studies show, however, that the deterioration in timing resolution is not large [13, 15].

The scintillator and PMT to be tested were placed in a cosmic ray telescope as shown in Figure 3, optically coupled using an UV-transparent grease GE Viscasil 60000. The cosmic ray events were selected by coincidence of the trigger counters with dimensions $2 \times 2 \times 1.2 \text{ cm}^3$ each. The reference counters positioned next to the trigger counters provided a measurement of the time that the cosmic ray passed through the test counter. All four reference and trigger counters were mounted on a trolley which could be positioned anywhere along the test counter.

The coincidence of trigger PMT pulses defined the TDC start time and generated a gate for the ADC. The ADC pedestal was measured every five minutes. Each pulse from the two reference PMT's and the two test PMT's was split and passed to both a LeCroy 2249A ADC and leading edge discriminators (LeCroy 623B and 4608C) whose output was sent to a LeCroy 2228A TDC calibrated to 50 ps/count. The discriminator threshold for the reference counters was chosen to be -30 mV , which is roughly 5% of the typical pulse height, in order to maximize acceptance. The threshold for the trigger counters was chosen to be -400 mV , which was roughly 1/3 of the typical pulse height in order to exclude background events.

3 Attenuation length

Figure 4 shows the pulse height distributions of the test counter PMT's. The trolley was positioned at the center. Results are shown for four different combinations of PMT's and counters: the XP2020/UR's at -2500V on the bulk counter, the R2021s on the bulk counter, the XP2020/UR's at -3000V on the 4 mm diameter fiber counter, and the XP2020/UR's at -3000V on the 2 mm fiber counter.

The effective attenuation length of each counter was measured by fitting a exponential function to the pulse height as a function of the distance from the each end of the counter. This gives two independent measurements for a single scan. Figure 5 shows the results obtained for the bulk counter, indicating an effective attenuation length of 160 cm. For the

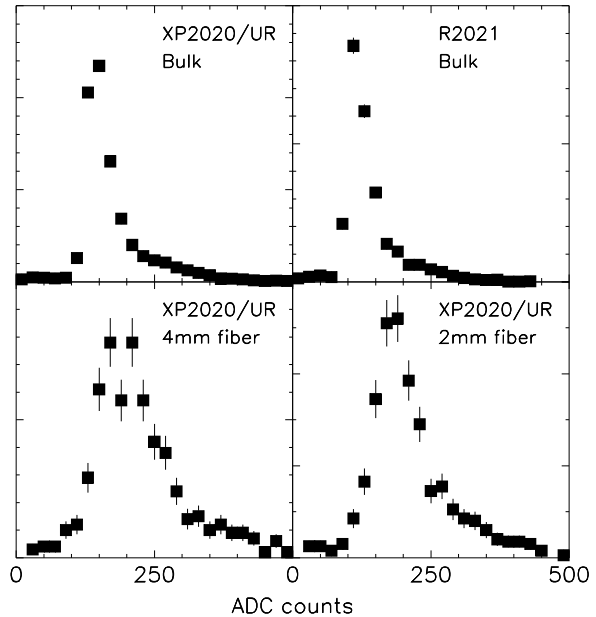


Figure 4: Distribution of ADC counts for a test counter photo multiplier (PMT3) for four different configurations: the XP2020/UR's on the bulk counter, the R2021s on the bulk counter, the XP2020/UR's on the 4mm fiber counter, and the XP2020/UR's on the 2mm fiber counter.

fiber counters, we find an effective attenuation length 168 cm for the 4 mm diameter fiber counter, and 147 cm for the 2 mm diameter fiber counter. Note that the effective attenuation length of the bulk counter is comparable to the effective attenuation lengths of the fiber counters. Thus, relative to the fiber counters, the bulk counter does not suffer from the loss of photon statistics at the locations far from PMT. As a result, the bulk counter may have an overall timing resolution superior to those of the fiber counters due to the better photon statistics, which we observe to be the case as reported below.

4 Timing resolution

In the following discussion, we assign the numbers 1 and 2 to the reference counter PMT's, 3 to the test counter PMT at $z = 0 \text{ cm}$, and 4 to the test counter PMT at $z = 100 \text{ cm}$. The mean time measured by the two reference counters is the time at which the cosmic ray crossed the test counter. The time measured by PMT i must be corrected to account for the time required for the pulse to reach the discriminator threshold (the 'time-walk' correction). The correc-

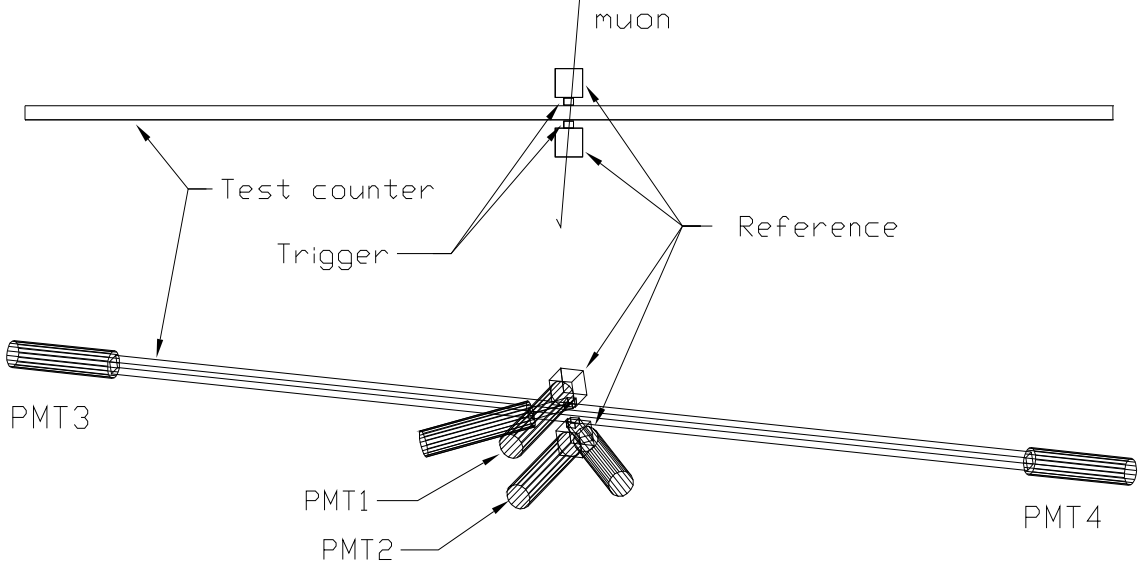


Figure 3: Cosmic ray telescope test setup.

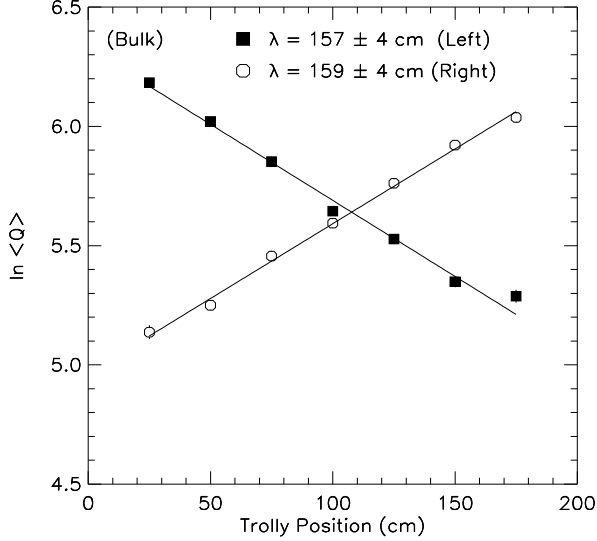


Figure 5: Attenuation length of the bulk counter, determined by fitting the mean pulse height from each end to an exponential.

tion has the form

$$T'_i = T_i - a_i Q_i^{-b_i}$$

where T_i is the measured TDC time and Q_i is the pedestal-subtracted ADC count. We use $b_1 = b_2 = 0.5$ for the reference PMT's. The constants a_1 and a_2 are determined from the data by minimizing the width of the distribution

$$T_{\text{ref-}} \equiv (T'_1 - T'_2)/2.$$

We collect data with the trolley placed at 25 cm intervals along the test counter, from $z = 25$ cm to $z = 175$ cm. We combine the data from all z positions and determine a single value for a_1 and for a_2 which is independent of z .

Using the values for a_1 and a_2 , we solve for the constants a_3, a_4, c_3 and c_4 of the test counter PMT's by minimizing the widths of the distributions

$$T_L(z) \equiv T'_3 - c_3 z - T_{\text{ref+}}$$

and

$$T_R(z) \equiv T'_4 - c_4 z - T_{\text{ref+}}$$

with

$$T_{\text{ref+}} \equiv (T'_1 + T'_2)/2.$$

The constant c_i is the inverse of the effective speed of light in the test counter and z is the distance to the PMT in question. Note in particular that the constants a_3 and a_4 are independent of z . We thus follow the method of calibration identical to the one used at the CLEO II detector where the beam crossing time is replaced by $T_{\text{ref+}}$. We do not require that $c_3 = c_4$ following the standard calibration technique of CLEO II. The value of the time-walk constant were chosen to be $b_3 = b_4 = 0.15$ as described later. We define the time resolutions of the left and right PMT's to be

$$\sigma_3(z) = \sqrt{\sigma_L^2(z) - \sigma_{\text{ref}}^2}$$

$$\sigma_4(z) = \sqrt{\sigma_R^2(z) - \sigma_{\text{ref}}^2}.$$

where $\sigma_L(z)$ and $\sigma_R(z)$ are the measured widths of $T_L(z)$ and $T_R(z)$, respectively. We then construct

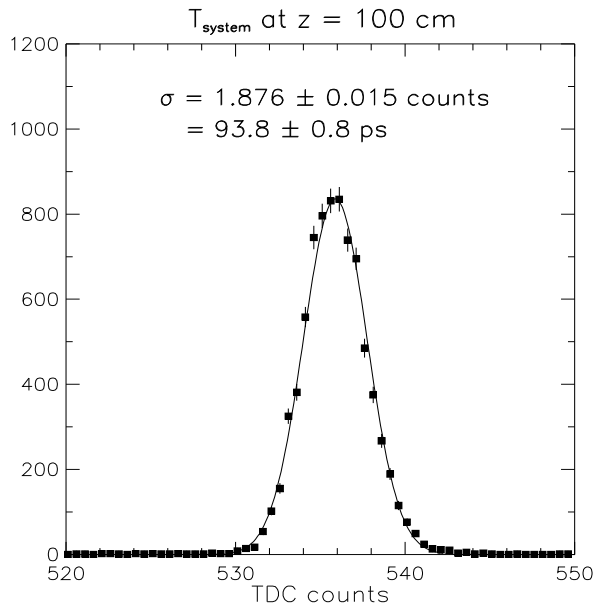


Figure 6: Distribution of T_{system} for the trolley at $z = 100$ cm, with the XP2020/UR's on the bulk counter. The reference counter resolution must be subtracted in quadrature from the width of this distribution to obtain $\sigma_{\text{tof}}(z = 100)$.

the weighted average of crossing time measurements as follows:

$$T_{\text{system}}(z) \equiv \frac{T_L(z)\sigma_4^2(z) + T_R(z)\sigma_3^2(z)}{\sigma_3^2(z) + \sigma_4^2(z)}.$$

The measured width of this distribution is denoted as $\sigma_{\text{system}}(z)$. Figure 6 shows T_{system} for the bulk counter at $z = 100$ cm, using XP2020/UR's. The distribution is well-described by a gaussian, and has a resolution of 94 ± 1 ps.

Finally, the contribution from the reference counters must be subtracted in quadrature to obtain the resolution of the test counter:

$$\sigma_{\text{tof}}(z) = \sqrt{\sigma_{\text{system}}^2(z) - \sigma_{\text{ref}}^2}.$$

In previous studies of similar time-of-flight systems, the resolution of the reference counter time difference $T_{\text{ref-}}$ was often taken to equal the average time $T_{\text{ref+}}$. However, such an assumption can be made only if the cosmic ray tracks have a narrow angular deviation and in the limit of small trigger counters. With our geometry, the angular acceptance of cosmic rays is approximately 20 degrees from vertical. This gives rise to a correlation between the two reference timings that cancels in $T_{\text{ref+}}$ but not in $T_{\text{ref-}}$ since when the track is close to one of the PMT's then it is away from

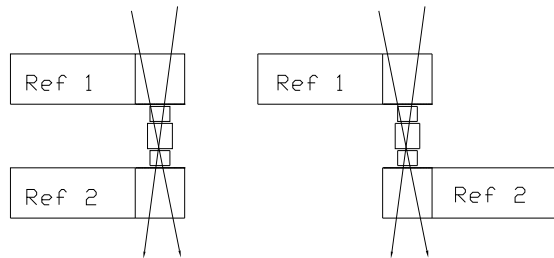


Figure 7: Reference counter configurations. The standard configuration (left), and that for the measurement of reference counter resolution (right). The effect of timing correlation between Reference 1 and 2 due to the track path for $T_1 + T_2$ in the left configuration is the same as that for $T_1 - T_2$ in the right.

the other (see Figure 7). Under these conditions, the resolution of $T_{\text{ref-}}$ is significantly greater than the resolution of $T_{\text{ref+}}$. There is also a smaller correlation introduced by the variation of the track position in the mid plane between the two trigger counters. In order to properly account for these correlations, the reference resolution was measured by placing PMT's facing opposite directions. The width of $T_{\text{ref-}}$ in this configuration should be equal to that of $T_{\text{ref+}}$ when both PMT's face the same direction. This assumption was verified by Monte Carlo studies [16]. The reference time resolution was thus measured to be $\sigma_{\text{ref}} = 59 \pm 1$ ps (Figure 8). Using this value of σ_{ref} , we obtain the resolution of the test counter system to be $\sigma_{\text{tof}} = 73$ ps at $z = 100$ cm. The contribution to σ_{tof} from the finite TDC bin size is negligible.

Having defined the timing resolution of the system, we examined the resolution obtained for different thresholds on the test counter discriminators. For this study, data were collected at $z = 100$ cm. The test counter discriminator thresholds were set to a fixed percentage of the average pulseheight for each end, and runs were taken for various thresholds in the range of 1% to 40% of the average pulse height. Figure 9 shows the resolution versus discriminator level for the bulk and the 4 mm fiber counters. The thresholds were chosen to be 5% for the 4mm fiber counter, and 10% for the bulk counter.

We next determined the value of the time-walk constants b_3 and b_4 constraining them to be equal. For this study data were collected for all z positions, and the simple average of $\sigma_{\text{tof}}(z)$ for all z position was calculated. Figure 10 shows how the average resolution depends on b_3 for the bulk and for the 4 mm fiber counter, each at their optimal discriminator thresh-

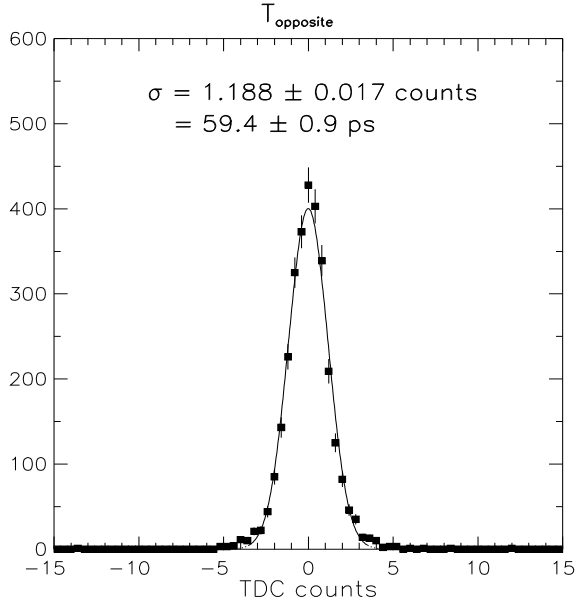


Figure 8: Resolution of reference counters, defined as the width of $T_{\text{ref}} = (T'_1 - T'_2)/2$ when the reference counter PMT's are oriented in opposite directions.

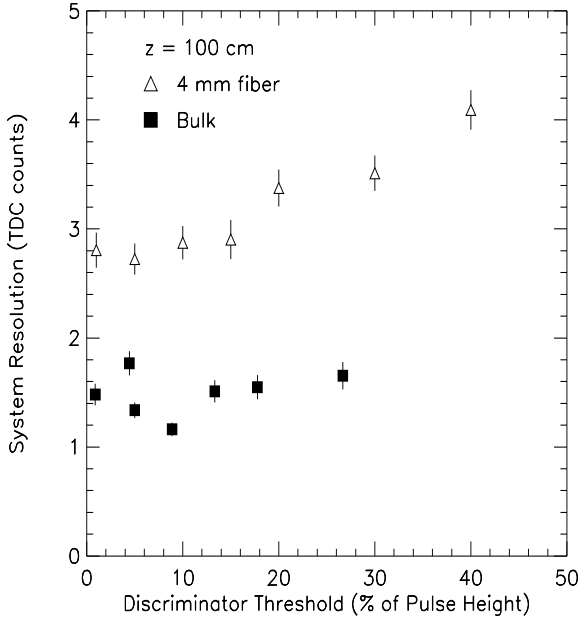


Figure 9: $\sigma_{\text{tof}}(z = 100)$ as a function of discriminator threshold for test counter PMT's: bulk counter (solid square) and 4mm diameter fiber counter (open triangle).

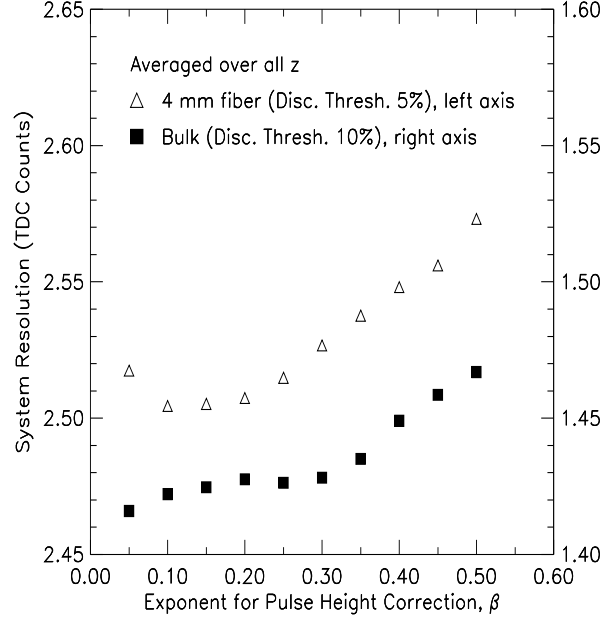


Figure 10: $\sigma_{\text{tof}}(z = 100)$ as a function of the exponential term of the test counter time-walk correction $b_3 (= b_4)$: bulk counter (right axis) and 4mm diameter fiber counter (left axis).

olds. The data favor lower values than the oft-used value of 0.5. We choose $b_3 = b_4 = 0.15$ for both fiber and bulk counters using the XP2020/UR's.

Figure 11 shows $\sigma_3(z)$, $\sigma_4(z)$, and $\sigma_{\text{tof}}(z)$ for the bulk counter using the XP2020/UR's. The left counter resolution was found to be worse than that of the right counter. This was found to be consistent with the photon statistics as measured and attributed to an imperfect optical coupling of the PMT to the scintillator block. We take the simple average of $\sigma_{\text{tof}}(z)$ to obtain an overall resolution of 71 ± 1 ps for the bulk counter. Figures 12 and 13 show similar data for the XP2020/UR's on the 4 mm diameter and 2 mm diameter fiber counters, respectively. We find an average σ_{tof} of 125 ± 3 ps for the 4 mm fiber counter and 133 ± 2 ps for the 2 mm fiber counters.

Lastly, we studied the bulk counter using Hamamatsu R2021 proximity-focus fine-mesh PMT's. For this study, we used the discriminator threshold at 10% of the pulse height. The optimal value for the constants b_3 and b_4 were found to be 0.30 using the method described earlier. Figure 14 shows $\sigma_3(z)$, $\sigma_4(z)$, and $\sigma_{\text{tof}}(z)$ for the R2021s on the bulk counter. The average σ_{tof} is found to be 81 ± 1 ps which is slightly worse than the resolution obtained by XP2020/UR. It should be noted, however, that the photocathode of R2021 covered only 65% of the end of the bulk scintillator and the difference is con-

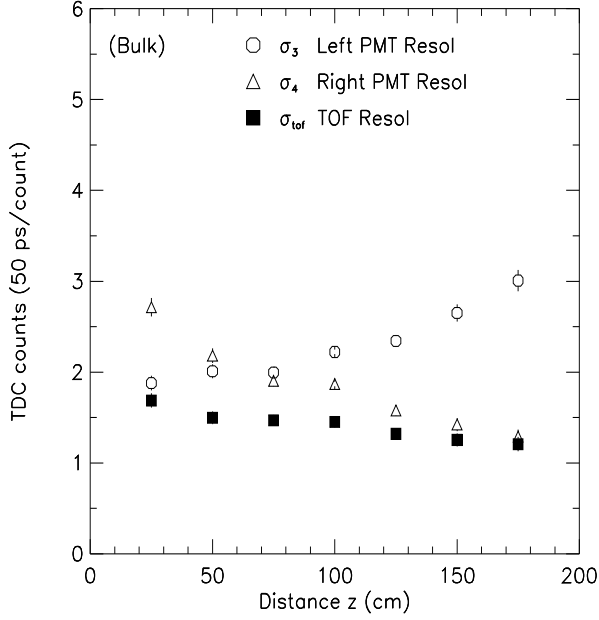


Figure 11: Time resolutions of the left PMT ($\sigma_3(z)$), the right PMT ($\sigma_4(z)$) and the weighted average ($\sigma_{tof}(z)$). For the bulk counter with XP2020/UR's.

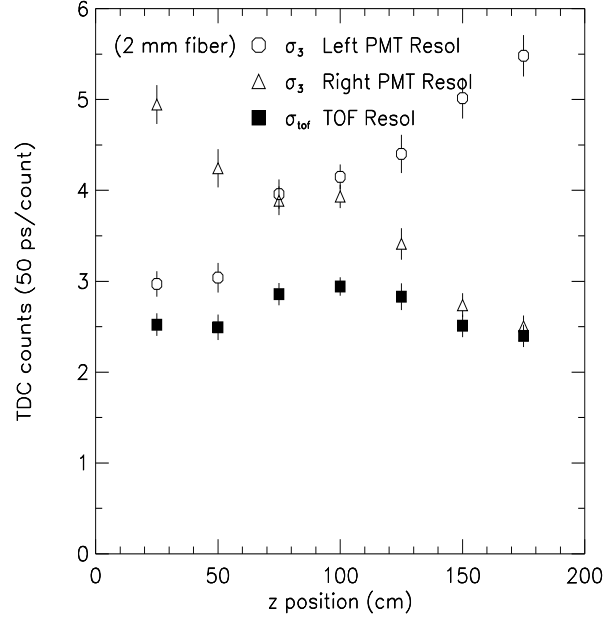


Figure 13: Time resolutions of the left PMT ($\sigma_3(z)$), the right PMT ($\sigma_4(z)$) and the weighted average ($\sigma_{tof}(z)$). For the 2 mm diameter fiber counter with XP2020/UR's.

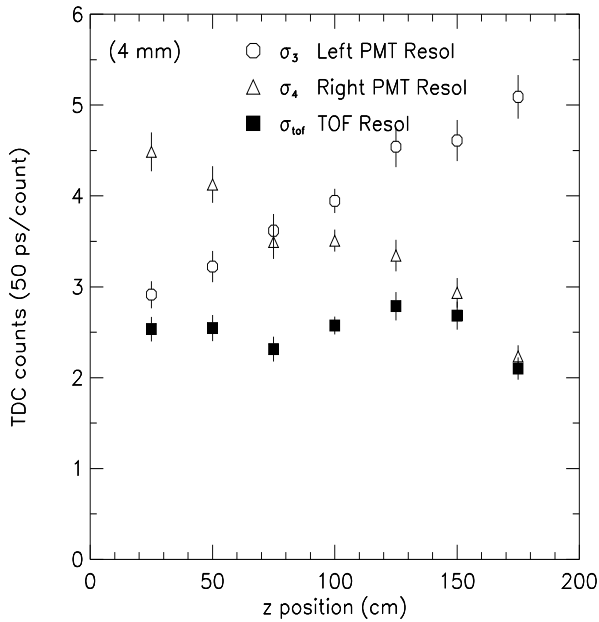


Figure 12: Time resolutions of the left PMT ($\sigma_3(z)$), the right PMT ($\sigma_4(z)$) and the weighted average ($\sigma_{tof}(z)$). For the 4 mm diameter fiber counter with XP2020/UR's.

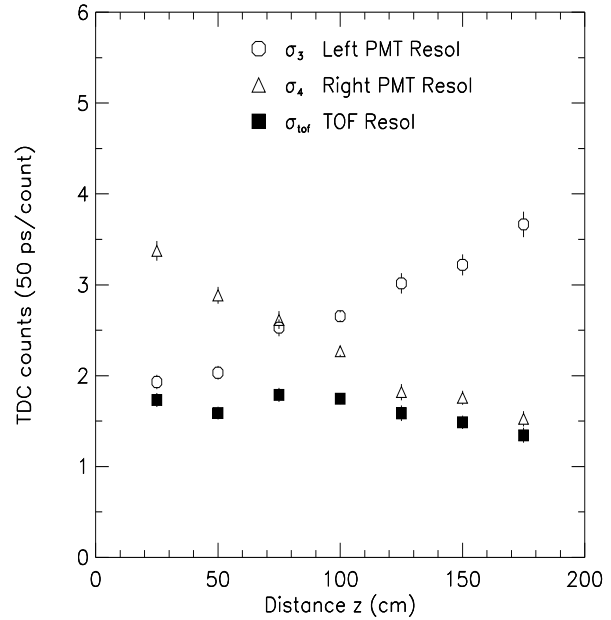


Figure 14: Time resolutions of the left PMT ($\sigma_3(z)$), the right PMT ($\sigma_4(z)$) and the weighted average ($\sigma_{tof}(z)$). For the bulk counter with R2021s.

Configuration	Resolution (ps)
XP2020/UR on bulk	71 ± 1
XP2020/UR on 4 mm fiber	125 ± 3
XP2020/UR on 2 mm fiber	133 ± 2
R2021 on bulk	81 ± 1

Table 1: The measured time resolution σ_{tof} for each configuration averaged over the length of the test counter.

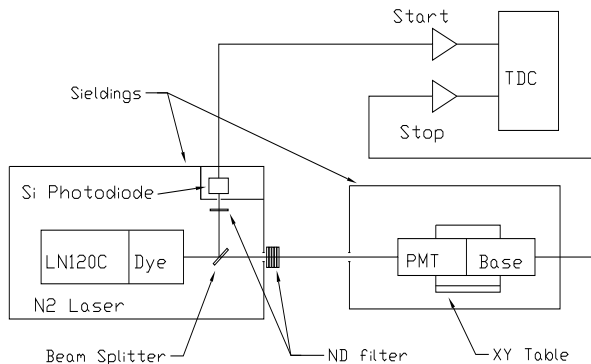


Figure 15: The setup for the single photon study. The entire system except the TDC logic is placed in a dark room.

sistent with the photons lost. Table 4 summarizes the average σ_{tof} for each configuration.

5 Single photon study

Examination of the single photon response of the XP2020/UR is instrumental in understanding one of the components of the time-of-flight system resolution. In particular, it is useful to know how the timing resolution varies according to the position on the photocathode at which the photon is incident. In addition, it also allows the gain of the PMT/base combination to be determined accurately. These are used as input parameters for the Monte Carlo simulation of the system.

The light source used for this investigation was a Laser Photonics LN120C nitrogen laser, which delivered pulses of wavelength 337.1 nm and r.m.s. duration 70 ps, each with 70 μJ , and at a repetition rate of about 10 Hz. After exiting the laser, the beam was split (see Figure 15). Figure 15. One beam triggered a fast photodiode (Newport 818 BB, with rise time < 200 ps) and defined the start time of the event while the other beam proceeded through a series of neutral

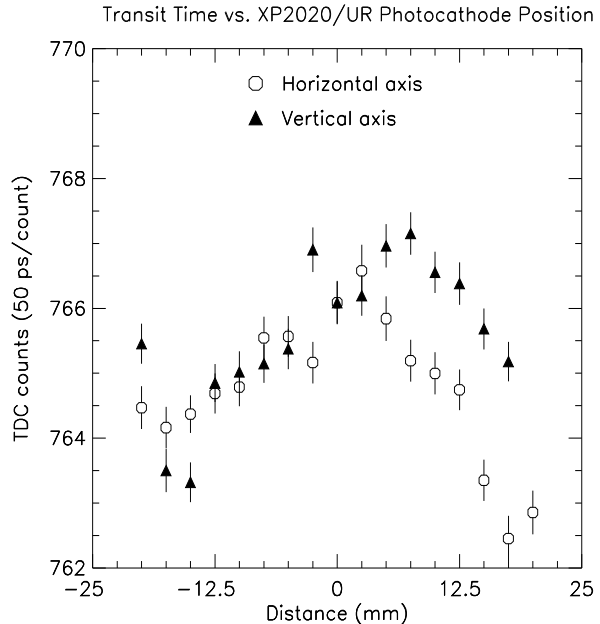


Figure 16: Transit time dependence on the location of the incident photon on the photocathode position for XP2020/UR.

density filters and then to the PMT. The attenuation provided by the filters was sufficiently large that a PMT pulse resulted only once for every ~ 10 laser pulses. Thus, approximately 95% of the signal events were due to one photoelectron.

The PMT was mounted on a movable x-y table which allowed the position of the incident photon to be varied across the photocathode. The PMT was magnetically shielded by mu metal inside degaussed soft iron. An iris with a 1 mm diameter aperture was placed in front of the PMT to define the beam size at the photocathode. The signal from the PMT was sent to a Mini-Circuits ZFL-1000LN amplifier and then split to an ADC and TDC. In order to shield the PMT from electrical noise generated by the laser, each of the two apparatus was separately enclosed in an electrically grounded box of 1/8 inch-thick aluminum.

The PMT was oriented such that longer dimension of the first dynode was horizontal. The repositioning of the stage was done in darkness to keep the PMT on and stable for the duration of the scan. A common pulse height correction was applied to all runs from the scans of both axes.

Figure 16 shows the mean TDC stop time for horizontal and vertical scans of the photocathode. We have observed that the shape of this curve depends on the potential applied to the accelerating grid G1. Figure 17 shows the mean corrected TDC stop time as a function of horizontal beam location for three

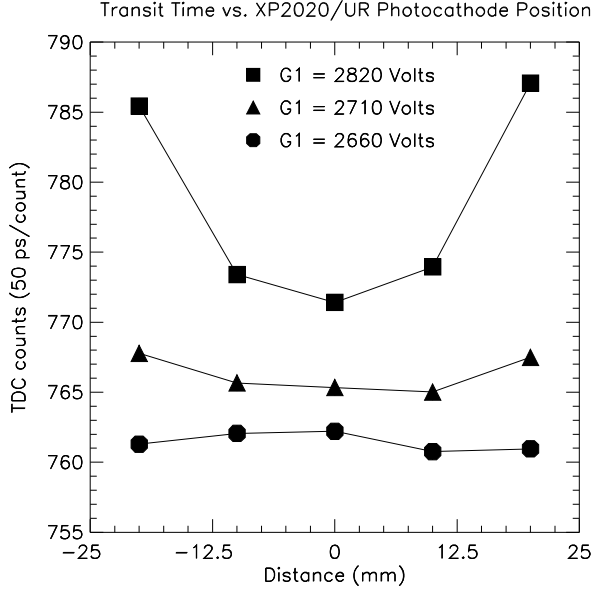


Figure 17: Transit time vs the location of incident photon on photocathode for XP2020/UR at -3000V . Plotted for three different potentials of the accelerating grid G1.

different G1 potentials. The position dependence of the transit time is clearly minimized for large potential differences between photocathode and G1. The variation of the shape with G1 potential suggests that the potential can be adjusted to provide a nearly uniform transit time for all photocathode positions, and that the resolution can be degraded if this parameter is not optimized.

The gain of each PMT/base combination was determined from the mean number of ADC counts measured per pulse, accounting for the 0.25 pC/count calibration of the ADC and for the splitter. The gain was measured at two different HV values, and found to vary as $(\text{HV})^n$ with n between 8.5 and 9.7. This is consistent with the dependence expected for a twelve stage PMT.

6 Monte carlo simulation

We developed a Monte Carlo program to simulate the performance of the system with the XP2020/UR PMT's on the bulk counter in order to understand the relative importance of the physical processes contributing to the resolution of the system.

Cosmic ray tracks were generated with a $\cos^2(\alpha\theta)$ angular distribution where θ is the polar angle with respect to the vertical. The coefficient $\alpha = 2$ was cho-

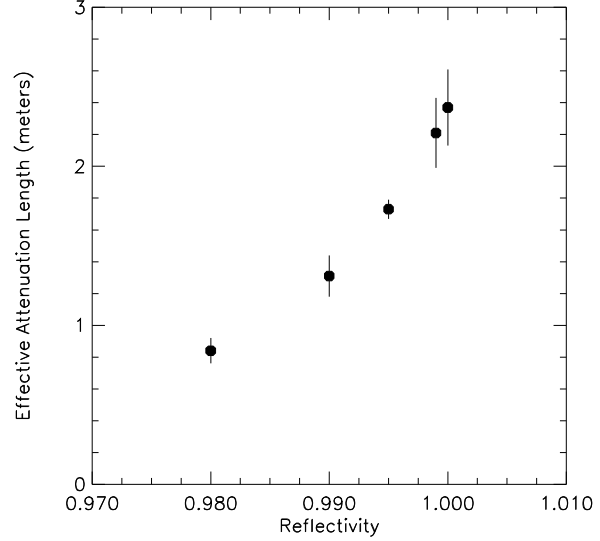


Figure 18: Monte Carlo effective attenuation length of bulk counter as a function of the reflectivity. The best estimate of reflectivity was taken to be 0.9925.

sen to match the shapes of the reference counter pulse height as described later. The number of photons was generated by the Landau distribution. The photon emission sites were distributed randomly along the length of the track, and the emission directions were isotropic. The decay time of the scintillator was taken to be 2.1 ns.

The path of each photon was traced through the scintillator until the photon either reached the PMT, or until it was lost by one of a number of different mechanisms. Photons were absorbed in the scintillator assuming a bulk attenuation length of 3.8 meters for BC-408. The index of refraction of BC-408 was taken to be 1.57 and the reflection/transmission at boundaries were modeled according to Fresnel's law for unpolarized light. Furthermore, the photon was assumed to be lost at the boundary with probability $1 - R$ due to imperfection. The photomultiplier window was modeled as a circular piece of glass with index of refraction 1.47 in direct contact with the scintillator. The quantum efficiency of the photocathode was assumed to be 26% averaged over the photon emission spectrum.

The reflectivity R was chosen as follows: The effective attenuation length of the bulk counter is a function of the reflectivity, the bulk attenuation length, and the geometry of the counter. Figure 18 shows the effective attenuation length as a function of the reflectivity. We chose $R = 0.9925$, which is the value that results in the measured effective attenuation length of 1.58 meters.

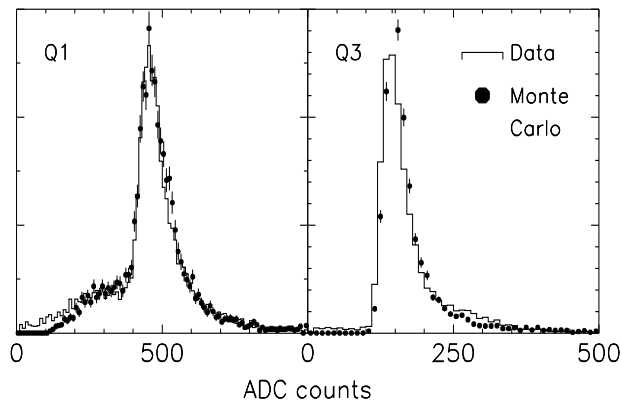


Figure 19: Comparison of Monte Carlo and data for the pulse height distributions of the reference counter (Q1) and the test counter (Q3). The horizontal scales are adjusted by roughly 20% to compare the shapes.

Two transit time effects were modeled. First, the transit time difference between center and edge of the photocathode was assumed to vary as r^2 . For the reference counter, we took this difference to be 250 ps. For the XP2020/UR, we took the results from Figure 16. Second, the transit time spread was modeled by a gaussian of sigma 250 ps.

The distribution of photoelectron arrival times was convoluted with a function which described the time response of the PMT to a delta function light input. For the test counter PMT's, this function was the pulse shape produced by the XP2020/UR on the single photon apparatus, measured by a 4 GHz Tektronix SCD5000 transient digitizer. For the reference counters, this function was a gaussian of width 1.5 ns.

The absolute yield of photons per unit path length was determined by requiring that the Monte Carlo pulse height distribution matches with the data distributions. We find a production rate of 5890 photons/cm. This corresponds to a BC-408 light output which is 20% of anthracene. Using the resulting pulse shape for each track crossing, the discriminator triggering time was defined to be the time the pulse shape crosses the threshold.

The pulse height distributions of the reference counter (Q1) and the test counter (Q3) are shown for Monte Carlo and data in Figure 19. The lower shoulder for the reference counter corresponds to tracks with large dip angle θ which intersect the sides of the reference counters. The coefficient α in the angular distribution $\cos^2(\alpha\theta)$ was determined to match the shape and size of this shoulder.

We calibrate the simulated data in the same way as described previously. We find $\sigma_{\text{tof}} = 55 \pm 3$ ps for the

(a) $\#\gamma/\text{cm}$	% of anthracene	σ_{tof} (ps)
1440	5	93 ± 6
2880	10	72 ± 6
5880 (nominal)	20	55 ± 3
8650	29	37 ± 7
11540	38	32 ± 9
23080	77	33 ± 5
(b) TTS (ps)		σ_{tof} (ps)
1000		91 ± 3
500		61 ± 4
250 (nominal)		55 ± 3
125		53 ± 5
0		52 ± 5
(c) Scintillation decay time (ps)		σ_{tof} (ps)
2.5		55 ± 6
2.1 (nominal)		55 ± 3
1.75		51 ± 6
1.5		48 ± 6
1.0		46 ± 7
0.0		40 ± 7
(d) Center/Edge difference (ps)		σ_{tof} (ps)
400		56 ± 4
300		55 ± 4
200 (nominal)		55 ± 3
100		57 ± 4
0		55 ± 4

Table 2: Monte Carlo study: Variation of the parameters in the simulation and the resulting change in $\sigma_{\text{tof}}(z = 100)$. The parameters varied are: (a) number of photons produced per unit path length of track also expressed as a percentage of anthracene output, (b) the XP2020/UR transit time spread, (c) the BC-408 decay time, (d) the XP2020/UR photocathode center/edge transit time difference.

$z = 100$ cm trolley position, in reasonable agreement with the data.

We varied a number of parameters in the Monte Carlo and observed the resulting changes in $\sigma_{\text{tof}}(z = 100)$. The parameters included the number of photons produced per unit length of cosmic ray track, the scintillator decay time, the transit time spread, and the photocathode center-edge difference of the transit time. In all cases, the variations were applied to the test counter and its PMT's, but not to the reference counters. Table 6 summarizes these results. We find that the resolution is limited primarily by photon statistics. In our application, the resolution is fairly insensitive to the transit time difference between photocathode center and edge. This is because only the central portion of the photocathode of XP2020/UR is used. In applications that use the entire photocathode, it will be critical to adjust the potential of G1 to make the transit time uniform across the photocathode surface.

7 Conclusions

We have measured the resolution of a small cross section prototype time-of-flight system. We find that a bulk counter manufactured to give an effective attenuation length comparable to a fiber counter gives a better resolution than the fiber counter due to the improved photon statistics. Results using magnetic-field-resistant photomultiplier tubes are comparable to those obtained with a fast photomultiplier of a more conventional design. We have studied the single photon response of XP2020/UR photomultiplier and found that the grid voltage adjustment is critical in flattening the distribution of transit time as a function of photon position on photocathode. This is particularly important if the entire photocathode is to be illuminated. We developed a detailed monte carlo simulation program which reasonably reproduces the data. The monte carlo shows that the critical element is the number of photoelectrons, emphasizing in particular the importance of the internal reflectivity of the scintillator block.

Acknowledgement

The authors would like to thank Ted Liu, Fay Shen, and technical staff at the high energy physics laboratory at Harvard University for the assistances at the early stage of the project. This work was supported by the department of energy grant DE-FG02-91ER40654.

References

- [1] See for example, J. S. Brown *et al.* (MARK III collaboration), Nucl. Instr. and Methods **221** (1984) 503; R. Heller *et al.* (ARGUS collaboration), Nucl. Instr. and Methods **A235** (1985) 26; J. M. Benloch *et al.* (DELPHI collaboration), Nucl. Instr. and Methods **A292** (1990) 319; G. C. Bonazzola *et al.* (OBELIX collaboration), Nucl. Instr. and Method **A356** (1995) 270.
- [2] W. B. Atwood, SLAC-PUB-2620 (1980).
- [3] Y. Kubota *et al.*, (CLEO collaboration), Nucl. Instr. and Methods **A320** (1992) 66.
- [4] R. T. Giles, F. M. Pipkin, and J. P. Wolinski, Nucl. Instr. and Methods **A252** (1986) 41.
- [5] Light guide can dramatically increase the path length dispersion, particularly when a large bending angle is used. See for example, T. Masam, Nucl. Instr. and Method **141** (1977) 251; G D'Agostini *et al.*, Nucl. Instr. and Method **185** (1981) 49.
- [6] G. D'Agostini *et al.*, Nucl. Instr. and Method **219** (1984) 495. The authors have archived a time resolution of 67 ps using a 2 m long scintillator block of thickness 15 cm.
- [7] H. Blumenfeld *et al.*, Nucl. Instr. and Method **A309** (1991) 169.
- [8] M. Kuhlen *et al.*, Nucl. Instr. and Method **A301**, (1991) 223. See also, A. Ferrer *et al.*, Nucl. Instr. and Method **A371** (1996) 397.
- [9] In a typical colliding beam experiment, one must also account for the finite size of the beam. For the CLEO detector, it introduces in quadrature an additional 30 ps uncertainty in the measured flight times.
- [10] G. Kittenring, Nucl. Instr. and Method **131** (1975) 451.
- [11] Bicon corporation, a private communication.
- [12] M. Kuhlen *et al.*, IEEE Trans. Nucl. Sci., Vol 38 (1991) 1052.
- [13] H. Kichimi *et al.*, Nucl. Instr. and Method **A325** (1993) 451. They report a transit time spread of 110 ps for no magnetic field and 130 ps for 1 Tesla field using Hamamatsu R2490-05 fine-mesh PMT.

- [14] G. Barbiellini *et al.*, Nucl. Instr. and Method **A362** (1995) 245; A. Antonelli *et al.*, Nucl. Instr. and Method **A368** (1996) 628; J. Jonath *et al.*, Nucl. Instr. and Method **A350** (1994) 221.
- [15] S. Ahmad *et al.*, Nucl. Instr. and Method **A330** (1993) 416. With Hamamatsu R3234-01 fine-mesh PMT on a 25 cm long scintillator, they measure a time resolution of 94 ps without magnetic field, and 109-115 ps with 0.5 Tesla field.
- [16] This technique does not account for the pulse-height correlation due to tracks with large dip angle which has short path lengths for both reference counters. Such pulseheight correlation couples to the timing correlation through the time-walk correction. Monte carlo studies indicate that we are underestimating the reference counter resolution by approximately 10%. To be conservative, we do not apply this correction.

Transit Time vs. XP2020/UR Photocathode Position

